The loading at ξ_n is given by

$$\gamma/V = f_n(\gamma_n/V) \tag{16}$$

The factor f_n differs from unity primarily near the leading edge $n = 1$, and secondarily near the trailing edge $n = N$. For $N = 10$, f_n varies as

n	1	2	3	4	5
f_n	1.128	1.009	1.003	1.001	1.000
n	6	7	8	9	10
f_n	1.000	0.999	0.998	0.995	0.977

For other N values, f_1 varies as,

N	1	2	3	4	5	10	15
f_1	1.103	1.123	1.127	1.127	1.128	1.128	1.128

The f_n factors can be applied directly to finite aspect ratio lifting surface theories that are based on elemental horseshoe vortices, constant vorticity panels, or for multiple load and downwash lines as in Ref. 2. In Ref. 2, a 2-line loading theory is derived for a load-line which can be any arbitrary function of the lateral coordinate. A $2N$-line theory (N load lines, N downwash lines) is the superimposition of the 2-line theory along the chord, distributed as in Fig. 1. The circulation at each of the N load lines is factored by f_n to obtain the chordwise loading at ξ_n.

References

[1] DeYoung, J., "Analytical Camber for Leading-Edge Droop," Vought Rept. 2-53340/OR-50724, May 1970, LTV Aerospace Corp., Dallas, Texas.

[2] DeYoung, J., "Calculation of Span Loading for Arbitrary Plan Forms," *Journal of the Aeronautical Sciences*, Vol. 22, No. 3, March 1955, pp. 208–210.

Effect of Unsteady Pressure Gradient Reduction on Dynamic Stall Delay

FRANKLIN O. CARTA*
United Aircraft Research Laboratories, East Hartford, Conn.

Nomenclature

a = dimensionless pivot axis location in semichords, positive aft
C_p = unsteady pressure coefficient
C_{ps} = quasi-steady pressure coefficient
F = real part of Theodorsen function
G = imaginary part of Theodoresen function
k = reduced frequency, product of semichord and frequency divided by velocity
S = pressure gradient ratio
t = time, sec
x = dimensionless chord position in semichords, positive aft
α = pitch angle, positive nose up, rad or deg
ω = pitching frequency, rad/sec
$( )^*$ = complex quantity
$\overline{( )}$ = time-independent quantity

Introduction

THE unsteady dynamic stall phenomenon has been the subject of a number of recent investigations. Of particular interest is the apparent delay in stall on an airfoil moving through the steady-state stall regime with positive angular velocity. This has been observed whether the airfoil is oscillating harmonically[1–3] or increasing its angle of attack monotonically.[4,5]

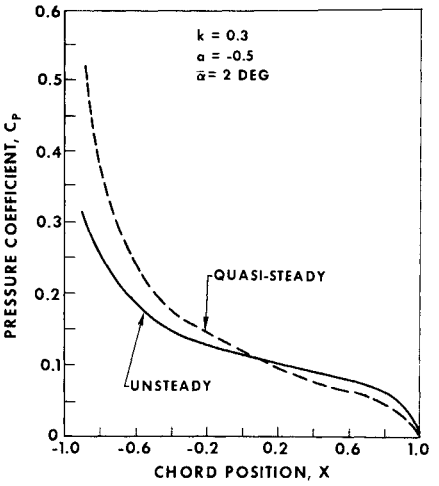

Fig. 1 Instantaneous pressure distribution at $\omega t = 11\pi/6$.

In a recent theoretical study Ham[6] was able to explain many of the features of moment reversal on an oscillating airfoil operating above the stall angle by postulating a continuously shed vortex sheet from the airfoil leading edge. However, he was unable to derive a criterion for the delay between the time the steady stall angle is exceeded and the time the vortex sheet begins to be shed. Isogai[7] has indicated that the delay is associated with the formation and movement of an unsteady separation bubble. However, one remaining unknown in his investigation is the way in which the separation bubble moves against the adverse pressure gradient without separating the boundary layer until well beyond the steady-state stall angle.

In this Note a possible theoretical mechanism for the delay in dynamic stall is discussed. The theory is confined to a comparison of the unsteady and quasi-steady chordwise potential flow pressure distributions. It is shown that the unsteady pressure gradient over the forward portion of the airfoil is less unfavorable than the steady pressure gradient. Hence, it can be inferred that a measurable stall margin exists for an unsteady motion relative to the steady state stalling angle, and that this stall margin increases with frequency.

Analysis

Theoretical pressure distributions

We can write the unsteady (or quasi-steady) pressure coefficient in the standard exponential form

$$C_p^* = \overline{C_p^*} e^{i\omega t} \tag{1}$$

where C_p is the pressure difference divided by the freestream dynamic pressure. The time-independent unsteady pressure coefficient, $\bar{C}_p^*$, for a pitching oscillation of amplitude $\bar{\alpha}$ is a complex function, reflecting the phase shift between pressure response and position. This is given by[8]

$$\bar{C}_p^* = 4\bar{\alpha}\{k^2[a - (x/2)](1 - x^2)^{1/2} + [F - kG(\tfrac{1}{2} - a)][(1 - x)/(1 + x)]^{1/2}\} + 4i\bar{\alpha}\{2k(1 - x^2)^{1/2} + [G + kF(\tfrac{1}{2} - a) - k/2][(1 - x)/(1 + x)]^{1/2}\} \tag{2}$$

where F and G are the real and imaginary parts of the Theodorsen function.[9] In the limit as $k \to 0$, Eq. (2) reduces to the quasi-steady form

$$\bar{C}_{p_s} = 4\bar{\alpha}[(1 - x)/(1 + x)]^{1/2} \tag{3}$$

It is assumed here that the motion is a harmonic function of time, given by

$$\alpha^* = \bar{\alpha} e^{i\omega t} \tag{4}$$

In an actual measurement on an oscillating airfoil the motion

Received May 24, 1971.
* Supervisor, Aeroelastics. Associate Fellow AIAA.

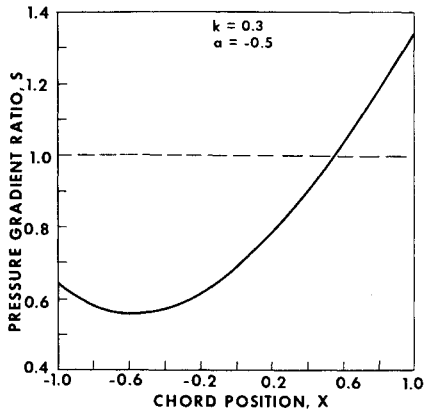

Fig. 2 Instantaneous pressure gradient ratio at $\omega t = 11\pi/6$.

will vary as the real part of Eq. (4)

$$\alpha = \bar{\alpha}\cos\omega t \tag{5}$$

and the corresponding measured unsteady pressure coefficient will be obtained by inserting Eq. (2) into Eq. (1) and taking the real part

$$C_p = 4\bar{\alpha}\{k^2[a - (x/2)](1 - x^2)^{1/2} + [F - kG(\tfrac{1}{2} - a)][(1 - x)/(1 + x)]^{1/2}\}\cos\omega t - 4\bar{\alpha}\{2k(1 - x^2)^{1/2} + [G + kF(\tfrac{1}{2} - a) - k/2][(1 - x)/(1 + x)]^{1/2}\}\sin\omega t \tag{6}$$

For comparison the quasi-steady measured pressure would be obtained by inserting Eq. (3) into Eq. (1) and again taking the real part

$$C_{p_s} = 4\bar{\alpha}[(1 - x)/(1 + x)]^{1/2}\cos\omega t \tag{7}$$

The critical point in the motion for stall delay occurs near the peak value of α for $\dot{\alpha} > 0$. From Eq. (5) this would lie in the range $5\pi/3 < \omega t < 2\pi$ (i.e., from 300° to 360° on a cosine wave, or from 30° to 90° on a sine wave), and for brevity here we choose the midpoint of the range, or $\omega t = 11\pi/6$, for our numerical example. (Similar results would be obtained for other points in this critical part of the motion.) In this case we have specified a quarter chord pivot axis ($a = -\frac{1}{2}$), a torsional amplitude of 2° ($\bar{\alpha} = \pi/90$ rad), and a reduced frequency of $k = 0.3$. In Fig. 1 the instantaneous unsteady pressure distribution for these conditions from Eq. (6) is plotted as a solid line, and the corresponding quasi-steady pressure distribution from Eq. (7) is plotted as a dashed line.

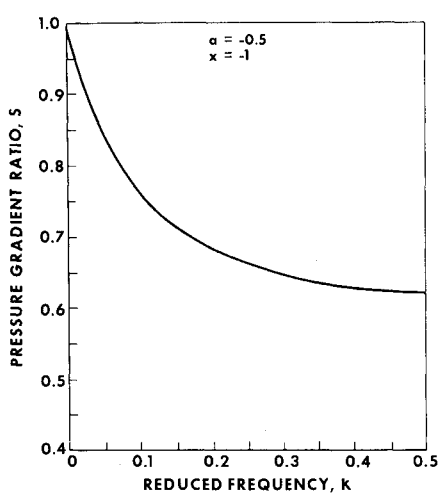

Fig. 3 Instantaneous pressure gradient ratio at $\omega t = 11\pi/6$ at the leading edge.

It is seen that over much of the chord the magnitude of the negative steady slope appears to exceed the magnitude of the negative unsteady slope, implying that the unsteady pressure gradient is less unfavorable than the steady pressure gradient.

Theoretical pressure gradients

To verify the assertion made above it is a simple matter to compute the derivatives of Eqs. (6) and (7) to obtain

$$dC_p/dx = [4\bar{\alpha}/(1 + x)(1 - x^2)^{1/2}]\{[k^2(x^2 - ax - \tfrac{1}{2}) \times (1 + x) - F + kG(\tfrac{1}{2} - a)]\cos\omega t + [2kx(1 + x) + G + kF(\tfrac{1}{2} - a) - k/2]\sin\omega t\} \tag{8}$$

$$dC_{p_s}/dx = -[4\bar{\alpha}/(1 + x)(1 - x^2)^{1/2}]\cos\omega t \tag{9}$$

If we divide Eq. (8) by Eq. (9) we can eliminate the leading and trailing-edge singularities and at the same time provide a direct comparison between the quasi-steady and the unsteady pressure gradient. This ratio is given by

$$S \equiv (dC_p/dx)/(dC_{p_s}/dx) = F - kG(\tfrac{1}{2} - a) - k^2(x^2 - ax - \tfrac{1}{2})(1 + x) - [G + kF(\tfrac{1}{2} - a) - (k/2) + 2kx(1 + x)]\tan\omega t \tag{10}$$

In the case of an unfavorable gradient near the leading edge, a value of $S < 1$ means that the unsteady pressure gradient is less unfavorable than the quasi-steady gradient.

This pressure gradient ratio is plotted vs chord in Fig. 2 for the same parameters used in Fig. 1. It is clear that over the forward 70% of the chord S is considerably less than 1, and in fact is approximately equal to 0.6 over the forward 50% of the chord. Now, assume that at this point in a quasi-steady motion an airfoil had just reached its separation point somewhere near the leading edge. The same airfoil reaching this point in an unsteady motion at $k = 0.3$ would have acting on its forward portion an unfavorable pressure gradient that was approximately 40% smaller than that which caused separation during the quasi-steady motion. Thus, we would expect the stall to be considerably delayed on the unsteady airfoil relative to the stall of the quasi-steady airfoil.

The effect of a variation in reduced frequency on S is shown in Fig. 3. Here Eq. (10) has been plotted vs k for the leading edge point, $x = -1$. It is seen that S decreases monotonically with k with the largest decrease taking place between $k = 0$ and $k = 0.2$. This implies that a significant stall delay would be possible even at low reduced frequencies, a phenomenon that has been observed many times in practice.

Conclusion

A quantitative prediction of the angular stall delay is beyond the scope of this short Note. Many unknown factors enter into such a computation including the variation in chordwise separation point with angle of attack and, more importantly, the unsteady boundary-layer response. A solution involving these considerations would be both difficult and nonlinear. Nevertheless, it is clear that the mechanism involved in dynamic stall delay is the large reduction of unfavorable pressure gradient during any unsteady motion.

References

[1] Carta, F. O. and Niebanck, C. F., "Prediction of Rotor Instability at High Forward Speeds. Vol. III. Stall Flutter," TR 68-18C, Feb. 1969, U.S. Army Aviation Material Labs., Fort Eustis, Va.

[2] Liiva, J., Davenport, F. J., Grey, L., and Walton, I. C., "Two-Dimensional Tests of Airfoil Oscillating Near Stall. Vol. I," TR 68-13A, April 1968, U.S. Army Aviation Material Labs., Fort Eustis, Va.

[3] Halfman, R. L., Johnson, H. C., and Haley, S. M., "Evaluation of High-Angle-of-Attack Aerodynamic-Derivative Data and Stall-Flutter Prediction Techniques," TN 2533, Nov. 1951, NACA.

[4] Fung, Y. C., *An Introduction to the Theory of Aeroelasticity*, Wiley, New York, 1955, pp. 452–453.
[5] Ham, N. D. and Garelick, M. S., "Dynamic Stall Considerations in Helicopter Rotors," *Journal of the American Helicopter Society*, Vol. 13, No. 2, April 1968, pp. 49–55.
[6] Ham, N. D., "Aerodynamic Loading on a Two-Dimensional Airfoil During Dynamic Stall," *AIAA Journal*, Vol. 6, No. 10, Oct. 1968, pp. 1927–1934.
[7] Isogai, K., "An Experimental Study on the Unsteady Behavior of a Short Bubble on an Airfoil During Dynamic Stall with Special Reference to the Mechanism of the Stall Overshoot Effects," Aeroelastic and Structures Research Lab. Rept. ASRL TR 130-2, June 1970, MIT.
[8] Postel, E. E. and Leppert, E. L., "Theoretical Pressure Distribution for a Thin Airfoil Oscillating in Incompressible Flow," *Journal of the Aeronautical Sciences*, Vol. 15, No. 8, August 1948, pp. 486–492.
[9] Theodorsen, T., "General Theory of Aerodynamic Instability and the Mechanism of Flutter," Rept. 496, 1935, NACA.

Thermal Buckling of Rotating Orthotropic Annular Plates

ERNEST B. UTHGENANNT*
United Aircraft Corporation, East Hartford, Conn.

Introduction

THE literature dealing with thermal buckling of circular plates is, indeed, very scarce. Mansfield[1] considered the buckling of a heated circular plate subjected to a temperature which varies parabolically in its plane. Sarkar[2] dealt with the buckling of a circular plate under inplane compression and subjected to temperature distributions along the radius and through the thickness of the plate. Bogdanoff, et al.,[3] determined whether a given radial temperature gradient will cause lateral buckling of a rotating disk. In this Note the thermal gradient required to cause buckling of a rotating orthotropic annular plate is calculated. The plate is also subjected to an external pull load applied at the outer periphery of the plate. A constant thickness plate is considered; however, the method described in this Note can easily be extended to include plates of variable thickness.

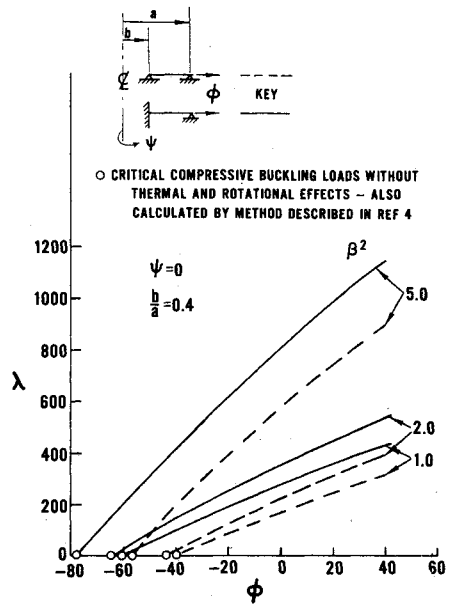

Fig. 1 Thermal buckling parameter vs in-plane loading parameter (neglecting rotational effects).

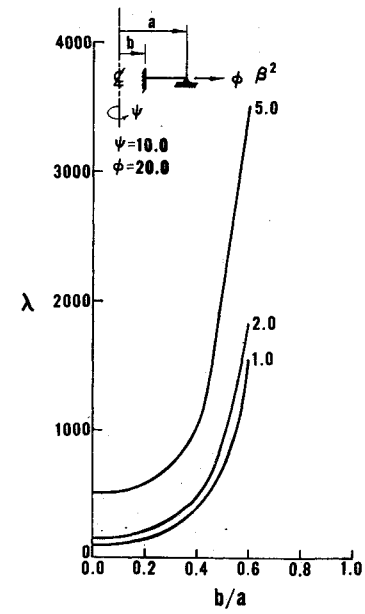

Fig. 2 Thermal buckling parameter vs b/a.

Analysis

The governing axisymmetric equation in terms of the deflection w and the stresses σ_r and σ_θ, including rotational effects, is

$$\Delta w = (h/D_r)(\sigma_r d^2w/dr^2 + \sigma_\theta(1/r)(dw/dr) + \gamma\omega^2 r dw/dr) \quad (1)$$

where

$$\Delta = d^4/dr^4 + (2/r)(d^3/dr^3) - \beta^2/r^2[d^2/dr^2 - (1/r)(d/dr)]$$

r,θ = radial and circumferential coordinates, respectively, $D_r = E_r h^3/12(1 - \nu_{r\theta}\nu_{\theta r})$, $\beta^2 = E_\theta/E_r$, E_θ, E_r = moduli of elasticity in the circumferential and radial directions, respectively, $\nu_{r\theta}, \nu_{\theta r}$ = Poisson's ratios, h = plate thickness, γ = mass density, ω = rotational velocity.

The stresses, including a parabolic radial temperature distribution and rotational effects, are given by

$$\sigma_r = C_1 r^{-1+\beta} + C_2 r^{-(1+\beta)} - r^2[(3 + \nu_{r\theta})\gamma\omega^2 + E_\theta \alpha g]/(9 - \beta^2) \quad (2)$$

$$\sigma_\theta = r d\sigma_r/dr + \sigma_r + \gamma\omega^2 r^2$$

where: α = coefficient of thermal expansion assumed to be directionally independent; g = temperature gradient coefficient; $\beta \neq 3$; C_1 and C_2 are determined from the loading conditions at the inner edge ($r = b$) and the outer edge ($r = a$).

Substituting the stresses into Eq. (1) and writing the resulting equation in nondimensional form gives

$$\nabla w - \frac{d^2w}{d\rho^2}(C_3\rho^{-1+\beta} + C_4\rho^{-(1+\beta)} - \rho^2\Psi) - \frac{dw}{d\rho}\left[\frac{\beta}{\rho}(C_3\rho^{-1+\beta} - C_4\rho^{-(1+\beta)}) - 3\rho\Psi\right] - \lambda\left(\rho^2\frac{d^2w}{d\rho^2} + 3\rho\frac{dw}{d\rho}\right) = 0 \quad (3)$$

where: $\nabla = \Delta$ with ρ substituted for r; $C_3 = C_1 a^{1+\beta} h/D_r$; $C_4 = C_2 a^{1-\beta} h/D_r$; $\Psi = (3 + \nu_{r\theta})\gamma\omega^2 h a^4/[D_r(9 - \beta^2)]$; $\lambda = E_\theta \alpha g h a^4/[D_r(9 - \beta^2)]$; $\rho = r/a$.

Received May 25, 1971.
* Assistant Project Engineer, Pratt & Whitney Aircraft Division; also Lecturer, University of Connecticut Graduate School Extension.